[1]T. Oka and T. Shimizu, Phys. Rev. A 2, 587 (1970).
[2]R. Karplus and J. Schwinger, Phys. Rev. 73, 1020 (1948).
[3]B. R. Mollow, Phys. Rev. A 4, 1666 (1971).
[4]A. Di Giacomo and S. Santucci, Nuovo Cimento 63B, 407 (1969); P. Bucci, P. Cavaliere, and S. Santucci, J. Chem. Phys. 52, 4041 (1970); P. Bucci, P. Cavaliere, S. Santucci, and A. M. Serra, Chem. Phys. Letters 5, 605 (1970); P. Bucci and S. Santucci, Phys. Rev. A 2, 1105 (1970); P. Bucci, M. Martinelli, and S. Santucci, J. Chem. Phys. 53, 4524 (1970).
[5]C. Cohen-Tannoudji, *Cargese Lectures in Physics* (Gordon and Breach, London, 1968), p. 347.
[6]W. Gordy and R. L. Cook, *Microwave Molecular Spectra* (Wiley, New York, 1970).
[7]A. Battaglia, A. Di Giacomo, and S. Santucci, Nuovo Cimento 43, 89 (1966).

PHYSICAL REVIEW A VOLUME 6, NUMBER 4 OCTOBER 1972

Hydrogenic-Carbon Lamb Shift Studied via Motional Electric Field Quenching of the $2\,^2S_{1/2}$ State

H. W. Kugel
Rutgers, The State University, New Brunswick, New Jersey* 08903
and Bell Laboratories, Murray Hill, New Jersey 07974

and

M. Leventhal and D. E. Murnick
Bell Laboratories, Murray Hill, New Jersey 07974

(Received 31 May 1972)

Beams of bare carbon nuclei were produced at 25 and 35 MeV using the Bell-Rutgers tandem Van de Graaff accelerator. Hydrogenic atoms, C^{5+}, were formed by electron pickup in dilute argon gas. About 2.2% of the C^{5+} beam is found to be in the metastable $2\,^2S_{1/2}$ state. On entering a magnetic field, the metastables are Stark quenched by the motional electric field $(\gamma/c)\,\vec{v}\times\vec{B}$. The quench-radiation decay length was determined by counting C^{5+} Lyman-α quanta as a function of distance traversed in the field. Windowless electron multipliers and thin-window gas-flow proportional counters were used to detect the 33.8-Å radiation. The decay length, as a function of field and energy was used to determine the Lamb shift ($2\,^2S_{1/2} - 2\,^2P_{1/2}$ splitting) with the aid of Bethe–Lamb quenching theory. The result is 780.1 ± 8.0 GHz. Corrections due to beam deflection, background, $2\,^2P_{3/2}$ state mixing, special relativity, and Zeeman effect are considered. Recent calculations are in agreement with the experimental result.

I. INTRODUCTION

Recent refinements in experimental and theoretical technique have removed several long-standing discrepancies in the predictions of quantum electrodynamics (QED). In particular, the hydrogen Lamb shift[1] ($\$ = 2\,^2P_{1/2} - 2\,^2S_{1/2}$ splitting) and the anomalous magnetic moment of the electron,[2] the two quantities whose discovery stimulated the reformulation of the theory, now stand in excellent agreement with experiment. Recent review articles[3,4] indicate that this satisfactory situation extends to essentially all other instances where the theory is applicable. In light of this overwhelming agreement between experiment and theory, justification for further work must be carefully investigated. In general, many fundamental reasons do exist for further tests of the validity of QED.[5] We mention here those reasons which specifically motivate the present experiment.

Lamb-shift measurements in high-Z hydrogenic atoms provide a basic test of our understanding of the virtual radiative processes associated with the electron and photon fields. These processes (e.g., the emission and reabsorption of virtual photons by the orbiting bound electron) which give rise to the Lamb shift are strongly affected by the external Coulomb potential. Experimental tests of the theory for systems in which the strength of this potential varies markedly from that of hydrogen, thus provide a basic and worthwhile test of QED.

The Lamb shift is given conventionally as a strongly Z-dependent expansion[6] in α and $Z\alpha$:

$$\$ = \sum_{i,j\geq 4} \alpha^i (Z\alpha)^j C_{ij} , \tag{1}$$

where Z is the nuclear charge, α is the fine-structure constant, and the C_{ij} are term coefficients, which are either independent, or slowly varying functions of Z. The higher-order coefficients become increasingly more difficult to calculate [terms of order $\alpha(Z\alpha)^6$ and $\alpha^2(Z\alpha)^4$ have been calculated to date]. It has been estimated that depar-

tures as large as a few tenths of 1% between experimental and theoretical s values may be observed in a $Z=10$ system because of the uncalculated terms in the expansion. Therefore, we concluded initially that even crude s measurements in high-Z systems are a significant test of the conventional theory and might at least force modification in calculational technique.

During the course of our work and motivated in part by it, Erickson has made a major improvement in the theory.[7] He has obtained a closed-form expression for the $Z\alpha$ part of the expansion in Eq. (1), thus removing the theoretical uncertainty associated with uncalculated higher-order terms in Z. For the case of C^{5+}, his result is about 0.1% higher than the conventional theoretical value. While the accuracy of this experiment is not sufficient to observe such a discrepancy, it is believed that experimental improvements and further extension of the technique to more highly ionized systems will enable a definitive test.

Table I illustrates the present satisfactory status of experimental and theoretical s values for $n=2$ state hydrogenic atoms. All experiments take advantage of the metastability of the $2\,^2S_{1/2}$ state against $E1$ decay which is forbidden because of the parity selection rule. The state decays relatively slowly by a second-order two-photon process. On the other hand, the $2\,^2P_{1/2}$ state does decay quickly in the electric dipole approximation with the emission of a Lyman-α quantum. Conventionally, the Lamb shift is determined by "quenching" low-energy metastable atoms via microwave mixing of the $2\,^2S_{1/2}$ and $2\,^2P_{1/2}$ levels.[8] Resonances are observed as transition frequencies between the Zeeman sublevels are tuned into coincidence with the frequency of an external generator. Accurate s values are obtained by measuring the fields and frequencies at which these resonances occur.

Extrapolation of the conventional atomic physics techniques to high-Z hydrogenics is extremely difficult. High energy is needed to strip off $Z-1$ electrons, implying the use of very hot plasmas or high-velocity atomic beams. In addition, a conventional Lamb-shift experiment on C^{5+} would require unreasonably high microwave power and frequencies, as well as unreasonably high-intensity magnetic fields.

We have employed a new high-velocity atomic beam method which is applicable to studies of many other highly ionized systems as well. Preliminary reports of our work have previously been published.[9,10] Our technique evolves from the innovative work of Fan, Garcia-Munoz, and Sellin[11] on Li^{2+}; but with important modifications. A beam of hydrogenic carbon atoms in the $2\,^2S_{1/2}$ state is produced using the Bell-Rutgers tandem Van de Graaff accelerator. A motional electric field then couples the $2\,^2S_{1/2}$ to the $2\,^2P_{1/2}$ state, which subsequently decays to the $1\,^2S_{1/2}$ ground state. Using time-dependent perturbation theory, the effective lifetime of the mixed state is shown to be a function of s, the unperturbed lifetime of the $2\,^2P_{1/2}$ state and the strength of the electric field. Lyman-α photons are detected as a function of position, and since the beam velocity is known, the lifetime is determined; hence s is obtained provided the other quantities are precisely known.

Similar experiments on highly ionized systems have been attempted by other workers,[12] but to our knowledge no other Lamb-shift results have yet been reported.

II. THEORY OF EXPERIMENTAL METHOD

A. Excited States

Figure 1 shows an energy-level diagram and the Z dependence of the associated level differences and widths for the low-lying levels of a hydrogenic atom with zero nuclear spin. Hydrogenic carbon ($^{12}C^{5+}$), with a nucleus having an even number of neutrons and protons ($I=0$) displays no hyperfine structure. The shift of the $2\,^2S_{1/2}$ level upward relative to the $2\,^2P_{1/2}$ level is the $n=2$ state Lamb shift (s) measured in this work. The Lamb shift breaks the degeneracy (from Dirac theory) of levels with the same J and to first order varies as $(\alpha Z)^4/n^3$. A recent calculation by Erickson[13] gives $s=783.68\pm0.25$ GHz for $^{12}C^{5+}$ ($n=2$). The $2\,^2P_{3/2}-2\,^2P_{1/2}$ fine-structure splitting (ΔE) is due mostly to the spin-orbit interaction and is given approximately by a Z^4 scaling of the hydrogen result. The $2\,^2P_{3/2}-2\,^2S_{1/2}$ energy difference is $\Delta E-s$. The $2\,^2P_{1/2}-1\,^2S_{1/2}$ energy difference (Lyman α) is given to lowest order

TABLE I. Lamb shift in GHz for the $n=2$ state of hydrogenic atoms. Theoretical values were privately communicated by G. W. Erickson and include his recent calculation of higher-order terms in $Z\alpha$. Experimental values are summarized in Ref. 1.

Species	s (theory)	s (expt)
H	1.057 91 ± 0.000 01	1.057 90 ± 0.000 06 1.057 77 ± 0.000 06
D	1.059 259 ± 0.000 028	1.059 28 ± 0.000 06 1.059 00 ± 0.000 06
He^+	14.044 78 ± 0.000 68	14.0454 ± 0.0012 14.0402 ± 0.0018
Li^{2+}	62.749 04 ± 0.0094	63.031 ± 0.327
C^{5+}	783.68 ± 0.25	780.1 ± 8.0 (present work)

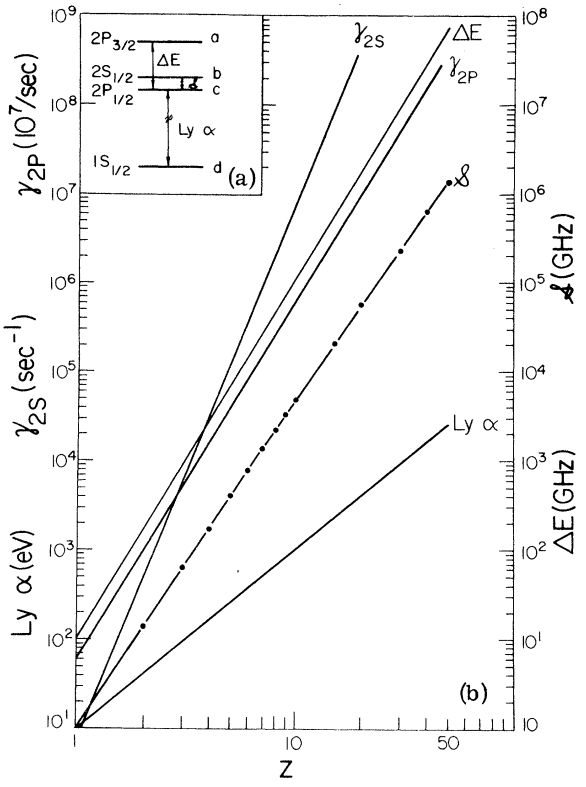

FIG. 1. (a) Partial energy-level diagram for the low-lying levels of a hydrogenic atom with zero nuclear spin. (b) Z dependence of the energy differences (ΔE, δ, Lyman-α) and widths (γ_{2S}, γ_{2p}) of the levels shown in inset (a).

by a Z^2 scaling of the hydrogen result. The energy differences for $Z=6$, $^{12}C^{5+}$ are $\Delta E = 14\,215.9$ GHz,[14] $\Delta E - \delta = 13\,432.2$ GHz and Lyman $\alpha = 367$ eV (33.8 Å).

B. Transition Rates

In the absence of perturbing fields, the $2\,^2S_{1/2}$ state is metastable. The parity selection rule forbids direct single-quantum $2\,^2S_{1/2} \rightarrow 1\,^2S_{1/2}$ $E1$, transitions. Single-quantum $E1$ decay to the $2\,^2P_{1/2}$ state is retarded by the small energy difference.[15] The dominant contribution to the spontaneous decay of the $2\,^2S_{1/2}$ state is two-photon decay to the ground state, in which the combined photon energies equal the energy-level difference. This decay rate has a Z^6 dependence and for $^{12}C^{5+}$, $\tau_{2S}^{spon} = 2.61$ μsec. Relativistic effects allow a single photon $M1$ transition direct to the ground state. The expression for the $2\,^2S_{1/2} \rightarrow 1\,^2S_{1/2}$ decay rate via these modes is[16]

$$\lambda_{2S}^{spon} = 8.2283Z^6 + 2.50\times10^{-6}Z^{10}\ \text{sec}^{-1}\ . \tag{2}$$

The $2P$ state decay rate via $E1$ transitions varies with a $(Z\alpha)^4$ dependence. The decay rate for the $2\,^2P_{1/2} \rightarrow 1\,^2S_{1/2}$ transition calculated in the dipole approximation is[17]

$$\lambda_{2p} = 6.265\times10^8 Z^4\ \text{sec}^{-1}\ . \tag{3}$$

Relativistic and QED corrections are expected to be of higher order[18] in $Z\alpha$.

C. Metastable Quenching

1. Two-Level Problem

Stark mixing of the $2\,^2S_{1/2}$ and $2\,^2P_{1/2}$ states in the presence of an electric field quenches the metastable state via a $2\,^2S_{1/2} \rightarrow 2\,^2P_{1/2}$ $E1$ transition. This transition rate is a function of the $2\,^2S_{1/2} - 2\,^2P_{1/2}$ energy difference and forms the basis for the indirect measurement of the Lamb shift described in this work. A first-order description of the decay rate, following Lamb and Retherford,[8] neglecting the presence of the higher-lying $2\,^2P_{3/2}$ state[19] follows.

Let $\psi(t)$ be the time-dependent wave function that characterizes the mixing of states b and c [refer to Fig. 1(a)] in terms of a superposition of their time-independent orthogonal wave functions U_b and U_c. E_b and E_c are the eigenvalues associated with U_b and U_c:

$$\psi(t) = b(t)\,U_b e^{-iE_b t/\hbar} + c(t)\,U_c e^{-iE_c t/\hbar}\ . \tag{4}$$

Substituting $\psi(t)$ into the nonrelativistic wave equation yields the equations of motion of first-order time-dependent perturbation theory:

$$\begin{aligned} i\hbar\,\dot{b}(t) &= V^* c(t) e^{-i\omega_{bc}t}\ , \\ i\hbar\,\dot{c}(t) &= V b(t) e^{+i\omega_{bc}t}\ , \end{aligned} \tag{5}$$

where $\omega_{bc} = E_b - E_c$ and V is the perturbing matrix element of the applied electric field:

$$V = \langle U_b \,|\, e\vec{\mathbf{E}}\cdot\vec{\mathbf{r}} \,|\, U_c\rangle = \sqrt{3}\ eEa_0/Z\ .$$

The above equations of motion do not include the finite spontaneous decay rates γ_b and γ_c. In order that

$$|b(t)|^2 \rightarrow e^{-\gamma_b t} \quad \text{and} \quad |c(t)|^2 \rightarrow e^{-\gamma_c t} \quad \text{as } V \rightarrow 0\ ,$$

decay terms are added to Eqs. (5) to give the correct phenomenological decay rate in the limit of zero perturbing field,[8] i.e.,

$$\begin{aligned} i\hbar\,\dot{b}(t) &= V^* c(t) e^{-i\omega_{bc}t} - \tfrac{1}{2} i\hbar\gamma_b b(t)\ , \\ i\hbar\,\dot{c}(t) &= V b(t) e^{i\omega_{bc}t} - \tfrac{1}{2} i\hbar\gamma_c c(t)\ . \end{aligned} \tag{6}$$

Eliminating the variable $c(t)$ and substituting the particular solution $b(t) = Ae^{ut}$ gives the following equation quadratic in u:

$$u^2 + u(i\omega_{bc} + \tfrac{1}{2}\gamma_b + \tfrac{1}{2}\gamma_c) + (i\omega_{bc}\tfrac{1}{2}\gamma_b + |V/\hbar|^2 + \tfrac{1}{4}\gamma_b\gamma_c) = 0\ , \tag{7}$$

with two roots

$$u_{1,2} = \frac{1}{2}\left(i\omega_{bc} + \frac{\gamma_b}{2} + \frac{\gamma_c}{2}\right)$$

$$\times\left[-1\pm\left(1-\frac{4(i\omega_{bc}\frac{1}{2}\gamma_b+|V/\hbar|^2+\frac{1}{4}\gamma_b\gamma_c)}{(i\omega_{bc}+\frac{1}{2}\gamma_b+\frac{1}{2}\gamma_c)^2}\right)^{1/2}\right]. \tag{8}$$

The variable term within the square-root factor is of the order of 10^{-3} for $^{12}C^{5+}$. In addition all terms of γ_b are at least $\sim 10^{-4}$ smaller than the next largest terms. Neglecting terms with γ_b and expanding the square-root factor gives

$$u_1=-\left(i\omega_{bc}+\frac{\gamma_c}{2}\right)+\frac{|V/\hbar|^2}{i\omega_{bc}+\frac{1}{2}\gamma_c}\,, \tag{9}$$

$$u_2=\frac{-|V/\hbar|^2}{i\omega_{bc}+\frac{1}{2}\gamma_c}\,. \tag{10}$$

The general solution to Eqs. (6) is

$$b(t)=A_1e^{u_1t}+A_2e^{u_2t}\,. \tag{11}$$

Applying the initial conditions $b(t=0)=1$ and $c(t=0)=0$ gives

$$A_1=u_2/(u_2-u_1)\,,\quad A_2=-u_1/(u_2-u_1)\,, \tag{12}$$

since $|A_1|^2\sim 10^{-6}$ and $|A_2|^2\sim 1$ for $^{12}C^{5+}$

$$|b(t)|^2\cong A_2A_2^*e^{(u_2+u_2^*)t}\,. \tag{13}$$

Therefore the decay rate of $b(t)$ is

$$\gamma=\frac{1}{\tau_{2_S}}=u_2+u_2^*=\frac{-\gamma_c|V/\hbar|^2}{\omega_{bc}^2+\frac{1}{4}\gamma_c^2}\,. \tag{14}$$

Thus, the Lamb shift ($\omega_{bc}=2\pi\,\delta_{bc}$) can be determined from a measurement of the quenched metastable decay rate γ in the presence of a known electric field given the width (γ_c) of the $2\,^2P_{1/2}$ state.

2. *Three-Level Problem*

A higher-order description of $2\,^2S_{1/2}$ metastable quenching in the presence of an electric field[11] includes the mixing of the $2\,^2P_{3/2}$ state. Similarly, starting with the time-dependent wave function

$$\psi(t)=a(t)U_a\,e^{-iE_at/\hbar}+b(t)U_b\,e^{-iE_bt/\hbar}+c(t)u_c\,e^{-iE_ct/\hbar} \tag{15}$$

yields the following simultaneous equations of motion from first-order time-dependent perturbation theory:

$$\begin{aligned}
i\hbar\,\dot a\,(t)&=Mb(t)\,e^{i\omega_{ab}t}-\tfrac{1}{2}i\hbar\gamma_a a(t)\,,\\
i\hbar\,\dot b\,(t)&=M^*a(t)\,e^{-i\omega_{ab}t}+V^*c(t)e^{i\omega_{bc}t}-\tfrac{1}{2}i\hbar\gamma_b b(t)\,,\\
i\hbar\,\dot c\,(t)&=Vb(t)e^{-i\omega_{bc}t}-\tfrac{1}{2}i\hbar\gamma_c c(t)\,,
\end{aligned} \tag{16}$$

where V and M are the perturbing matrix elements of the applied electric field:

$$\begin{aligned}
V&=\langle U_c\,|\,e\vec{\mathbf{E}}\cdot\vec{\mathbf{r}}\,|\,U_b\rangle=\sqrt{3}\,eEa_0/Z\,,\\
M&=\langle U_a\,|\,e\vec{\mathbf{E}}\cdot\vec{\mathbf{r}}\,|\,U_b\rangle=\sqrt{6}\,eEa_0/Z\,.
\end{aligned} \tag{17}$$

The above time-dependent equations of motion include damping terms to give the expected phenomenological decay rates (γ_a, γ_b, γ_c) in the limit of zero perturbing electric field ($V\to 0$, $M\to 0$).[8] A procedure similar to that given above yields

$$\gamma(2\,^2S_{1/2}\to 2\,^2P_{1/2})=\gamma_c\left(\frac{|V/\hbar|^2}{\omega_{bc}^2+\frac{1}{4}\gamma^2}+\frac{|M/\hbar|^2}{\omega_{ab}^2+\frac{1}{4}\gamma^2}\right)\,, \tag{18}$$

where $\gamma_c=\gamma_a$. The $|M/\hbar|^2$ term for $^{12}C^{5+}$ contributes $\sim 0.5\%$ while higher-order terms are smaller by at least $\sim 10^{-2}$.

D. Motional Electric Field

There are numerous experimental difficulties associated with generating and accurately measuring the large uniform electric fields needed to produce measurable decay lengths for high Z metastable ions moving at relativistic velocities. These difficulties were avoided by employing the effective motional electric field that results from the application of a magnetic field B transverse to the direction of an ion moving with velocity v. Transforming the applied magnetic field to the rest frame of the moving ion gives fields effective at the ion of $\vec{\mathbf{E}}_m=\gamma'(\vec{\mathbf{v}}/c)\times\vec{\mathbf{B}}$ and $\vec{\mathbf{B}}_m=\gamma'\vec{\mathbf{B}}$, where $\gamma'=[1-(v/c)^2]^{-1/2}$. Thus, an applied transverse magnetic field of 3 kG generates an effective electric field (~ 60 kV/cm) sufficient to reduce the $^{12}C^{5+}$ metastable decay length to about 2.8 cm at 25 MeV.

III. EXPERIMENTAL TECHNIQUE

A. Apparatus

1. *Ion Source and Accelerator*

Metastable C^{5+} beams were initiated by extracting 20-keV C^- beams from the duoplasmatron-hydrogen exchange ion source, of the Rutgers-Bell tandem Van de Graaff accelerator (Fig. 2). Convenient injection currents of 0.5–1 μA were obtained using ion-source gas mixtures of carbon monoxide or methane and hydrogen. Injected C^- ions were accelerated through potentials (U) of ~ 5 or ~ 7 MV to the terminal of the tandem Van de Graaff and stripped with a 10-μg/cm^2 carbon foil to equilibrium charge-state fractions[20] of approximately 18% (C^{3+}), 62% (C^{4+}), 19% (C^{5+}), and 1% (C^{6+}) at 5 MV or 6% (C^{3+}), 60% (C^{4+}), 31% (C^{5+}), and 3% (C^{6+}) at 7 MV. These ion species (of charge q) were further accelerated to ground potential obtaining a total energy of $(q+1)U$. After focusing, the beam passed through a post stripper foil located midway between the accelerator's output terminal and its 90° analyzing magnet (see Fig. 2). The post stripper device allowed up to 14, 10-μg/cm^2 carbon stripper foils to be inserted individually into the beam. Viewing ports permitted visual inspection of the working foil during runs. The C^{6+} component, resulting from stripping the

dominant C^{4+} beam at 25 or 35 MeV, was selected with the 90° analyzing magnet from the various energy and charge-state components emerging from the post stripper foil. The analyzing magnetic field monitored with an NMR gaussmeter probe provides the primary energy determination. The analyzed beam of bare carbon nuclei was focused, collimated, and steered for a distance of about 12 m through a beam pipe evacuated to an average pressure of 1×10^{-6} Torr to a baffled windowless gas cell which typically contained argon at a pressure of 0.1 Torr. The gas cell consisted of a 10.16-cm-long cylinder, 5.08 cm in diameter with a needle value for gas input and a thermocouple pressure gauge. Baffling was accomplished with a series of 18 disks 0.4 mm thick with 0.317-cm center holes, separated by 0.28-cm spacer rings. Baffling with such a series of disks minimized small-angle multiple scattering of the beam as well as gas escaping from the center cylinder. The gas cell and baffle section were insulated to monitor beam current lost. With optimal focusing, about half the total beam current was lost in this system. The dominant

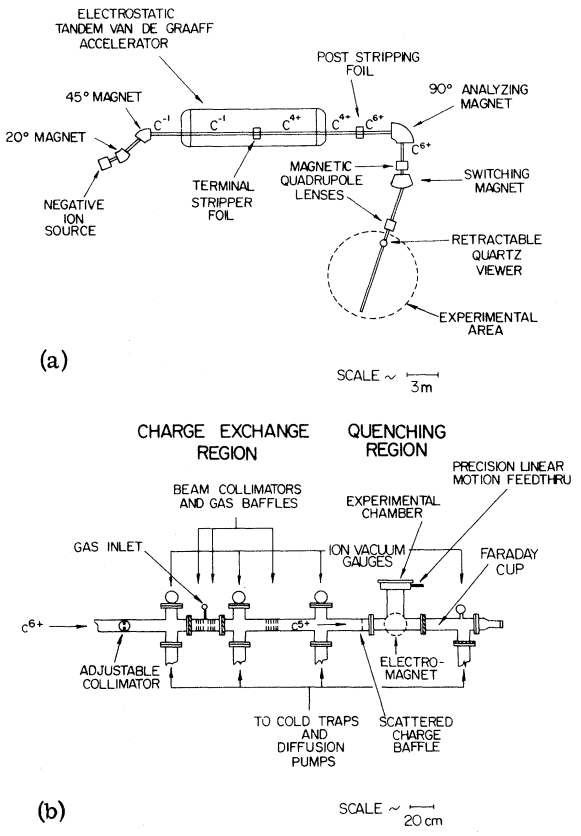

FIG. 2. (a) Schematic representation of the accelerator and experimental areas. (b) Schematic representation of the experimental apparatus.

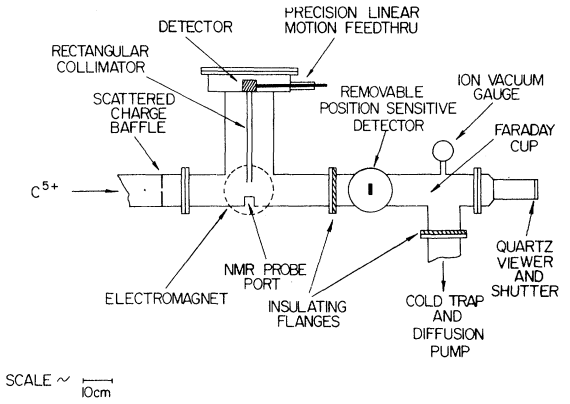

FIG. 3. Schematic representation of the quenching chamber and Faraday cup.

charge-transfer process occurring in the gas cell was found to be (as discussed in Sec. III A 2) one electron pickup by bare carbon nuclei.

2. *Quenching Chamber*

The beam emerged from the gas cell with a C^{5+} ($2\,^2S_{1/2}$) component and traversed a distance of about 2 m through additional collimators and gas baffles into a differentially pumped quenching region maintained at a pressure of $\sim 2\text{–}3\times10^{-7}$ Torr.

In the quenching region [see Fig. 2(b)], a "6-in." Varian electromagnet was used to apply transverse magnetic field intensities of 2000–3325 G. The magnet pole faces were pressed against the flat parallel sides of the 0.635-cm-thick aluminum chamber walls. Figure 3 shows the details of the experimental chamber geometry. The magnetic field intensity was monitored with an NMR probe mounted outside the chamber in a port, 2 cm from the beam axis. The NMR spectrometer system allowed a determination of both the stability and absolute magnitude of the applied field.

The 33.8-Å (367-eV) Lyman-α quench radiation was monitored with detectors mounted in a subchamber above the quenching region and positioned so as to allow motion parallel to the beam.

3. *Windowless Electron Multipliers*

Initially, windowless Spiraltron electron multipliers were employed as detectors. The pulse heights of the detector output signals were approximately constant and therefore provided no energy information. The detectors were typically operated at ~ +800-V bias and were conditioned to minimize detector noise by operating with applied bias in pressures of $\sim 2\text{–}3\times10^{-7}$ for about 24–48 h prior to each run. The average pulse heights of signals associated with Lyman-α photons were greater than those attributed to detection system

noise. Hence, the detector output signals were sent to a single-channel pulse-height analyzer operated in the integral mode and set to optimize the signal-to-noise ratio. The output of the single-channel analyzer was sent to a scaler for counting. The detector viewed the beam through a 15.2-cm-long rectangular cross section (1.11 cm wide by 0.79 cm long) brass collimator. The end of the collimator was 2 cm above the undeflected beam axis. The rectangular cross section helped to minimize changes in detection solid angle due to possible small transverse displacements of the beam. A 1000-Å Parylene-C filter[21] (12.9 $\mu g/cm^2$ with approximately 75% transmission at 367 eV) was glued to a frame with silicone rubber cement and positioned over the input to the rectangular collimator. The filter served as a barrier to low-energy charged particles and reduced detection efficiency for very-low-energy photons. The detector was mounted on a carriage assembly that could be positioned reproducibly over a distance of 5.08 cm along the beam axis by means of a precision feed-through micrometer. This detection system was used to accumulate about 70% of the presented data.

4. *Proportional Counter*

Recently, a thin-window gas-flow proportional counter was constructed to enable energy resolution and increase detection efficiency. The detector chamber is 10.76 cm long and 3.77 cm in diameter. The center wire is 0.0076-cm-diam first drawn carbon quartz. Gas flowed through the counter chamber via ports at each end. The window was inserted on a circular frame into a port in the detector wall. The window frame pressed against an O-ring seal to maintain a pressure-vacuum seal. The window requirements were (a) high transmission at 33.8 Å to optimize the signal-to-background ratio, (b) sufficient tensile strength to sustain pressure differentials of at least 150 mm Hg, and (c) low gas permeability to retard leakage of counter gas into the quenching region of the experimental chamber where pressures were maintained at $2-3\times10^{-7}$ Torr. These requirements were met using 3000-Å Parylene-C film.[21] The Parylene-C was mounted on 82% transmission, 40-wire/cm electroformed nickel support mesh. The support mesh was on the vacuum interface side of the window. A 97% transmission, 8-wire/cm electroformed nickel mesh was placed on the interior side of the Parylene-C to provide electrical conductivity across the window as an aid to charge collection. Parylene-C film and nickel meshes were bonded to the brass window frame with silicone rubber adhesive. The counter gas was 90% argon and 10% methane (*P*-10) maintained at typical pressures of 70 mm. The proportional counter and experimental chamber were evacuated simultaneously before filling the proportional counter in order to reduce pressure differentials across the window. The detector viewed the beam through a 32.4-cm-long rectangular cross-section (1.11×0.79 cm), brass collimator. The input end of the collimator was 2 cm above the undeflected beam. The detector was mounted on a carriage assembly that could be positioned reproductably by means of a precision linear motion feed-through micrometer.

The counter was operated with about +800 V on the center wire. The output signal was connected to an FET preamplifier placed outside of the experimental chamber. Preamplifier signals were fed to a variable time constant linear pulse-shaping amplifier adjusted for optimum energy resolution. The shaped pulses were processed by an analog-to-digital converter and displayed using an on-line computer system. The computer code allowed for preliminary on-line data analysis and recording of the data on magnetic tape.

5. *Faraday Cup*

After the beam emerged from the quenching region, it entered a section of electrically insulated beam pipe which served as a beam stop and Faraday cup for monitoring the beam intensity (see Fig. 3). The Faraday cup was connected to a digitizing current integrator. Beam currents of ~10–15 nA (charge current) were observed. Digital output pulses from the current integrator were counted with a scaler. In addition, the insulated Faraday cup section of beam tube provided a quartz viewer (with a removable conducting shutter) for observing beam alignment and a side port that permitted insertion of a silicon position-sensitive particle detector. This allowed for charge state analysis of the beam using the magnetic field in the quenching region as discussed below.

B. Procedure

1. *Metastable Beam Formation*

The experimental technique employing electron pickup by bare carbon nuclei was chosen for C^{5+} $2\,^2S_{1/2}$ metastable ion production rather than the method of stripping multiply charged ions because of the *a priori* expectation that this would result in the cleanest and least ambiguous measurement situation. Minimum background and maximum formation of the metastable state were expected.

At a given particle energy, it is well known that the equilibrium ionic charge on passing through a foil is greater than the equilibrium charge through an equal mass density of gas.[22] The energies at which these experiments were run were chosen so that C^{6+} would be the major beam constituent

emergent from the post stripper foil, and a large fraction of the C^{6+} ions would be converted to C^{5+} in the adder gas with minimal two-electron pickup.

The electron-pickup process enhances $2\,^2S_{1/2}$ metastable state formation. S states are favored in pickup whereas high angular momentum states are preferentially formed in stripping.[23] The cross section for electron pickup to S states of principal quantum number n is expected to be proportional to n^{-3}.[24] We estimate that any S states below $n = 20$ decay before reaching the quench region.

The C^{6+} ions (bare carbon nuclei) at the desired energy were obtained by first selecting the direct C^{4+} component at ~25 or ~35 MeV with the 90° analyzing magnet. The post stripper foil was then inserted into the beam and the analyzing magnetic field was adjusted proportionally to obtain C^{6+} at the same energy. Another reason for selecting the C^{6+} component, rather than hydrogenic C^{5+}, was that quenching in the analyzing magnetic field, as well as the other focusing fields, would completely depopulate any C^{5+} $2\,^2S_{1/2}$ metastable state before the ions reached the experimental area. The possible presence of ionic species (from residual gas impurities in the accelerating system) with a magnetic rigidity comparable to that of 25 or 35 MeV C^{6+} was investigated by observing analyzed beam current as a function of terminal potential and magnetic field. No nearby beams were found, and the intensity of any impurity beam within ± 20 keV of the desired beam energy was less than 0.01%.

2. Beam Energy

The mean beam energy was determined from calibrations based on well-known proton induced standard nuclear reactions performed routinely and reproducibly in other experiments at the tandem laboratory. The thresholds of these induced nuclear reactions are used to relate the proton energy and the field of the 90° analyzing magnet for a fixed radius of orbit curvature as determined by collimating slits. This same radius of curvature and the calibrated magnetic field determine the energies of the C^{6+} beams. The beam energy enters into the analysis for s as the fourth root which, as is discussed in Sec. IV, makes the effect of the energy uncertainty negligibly small relative to other experimental uncertainties.

3. Beam Alignment

Stringent beam and detector alignment procedures were followed to ensure an accurately defined and reproducible experimental geometry. The quartz viewer, at the end of the Faraday cup, permitted beam alignment to be determined with the detection chamber under the actual experimental vacuum conditions. Typically, both the parallelism of the magnet pole faces and the detector motion relative to the beam axis were checked before each run. An input quartz viewer with an aperaturelike reference marking was inserted into the beam about 3 m in front of the gas cell (see Fig. 2). The system alignment was checked by viewing the beam fluorescence stopping position on the input quartz viewer with a telescope which focused through the Faraday cup quartz viewer, through the rectangular quenching chamber, the various collimators, the gas cell baffles and the positioning slits. These elements were centered on the telescope line and subsequently determined the beam position. The detector's rectangular aperature could also be observed with the same telescope setting allowing checks of the detector motion relative to the beam axis. The beam was typically about 3 mm in diameter with a maximum transverse position uncertainty of ± 1.5 mm.

4. Charge-State Analysis

The carbon ionic states emerging from the gas cell were studied using a highly collimated beam (of less than 1 pA) with a position-sensitive detector inserted into the beam beyond the homogeneous transverse magnetic field. The applied field was adjusted to allow simultaneous observation of the individual charge-state intensities with the position sensitive detector. The magnetic field could also be adjusted to allow the individual charge-state components to be viewed simultaneously on the quartz viewer at the end of the Faraday cup as a consistency check. Charge states were studied as a function of beam energy, gas type, and gas pressure. The results of these studies are given in Sec. IV.

5. Transverse Magnetic Field

The homogeneity of the applied transverse magnetic field was determined by observing the magnetic field intensity as a function of position along the beam axis using an NMR gaussmeter probe. Homogeneity measurements were made using an apparatus that allowed an NMR probe to be positioned accurately and reproducibly along the beam axis in the experimental chamber. The homogeneity was corrected to ~0.01% by shiming the magnet. The fringing-field intensity, or the field intensity along the beam axis prior to the detection region was determined using a Hall-effect probe. The calibration for the off-axis position of the NMR gaussmeter probe was made by comparison with the field intensity at the beam axis. The absolute value of the applied magnetic field was determined from the probe-position corrected NMR resonant frequency. The typical correction

was 0.2% in field.

6. Data Collection

Measurements were made at ~25 and ~35 MeV for applied magnetic field intensities from 2000–3325 G and for opposite field directions (normal and reverse). Data were taken over a distance of 5.08 cm, at 11 counting positions each 0.508 cm apart, for fixed amounts of integrated beam current. The effects of any small systematic trends with time were minimized by following a sequence of counting positions that began at the middle of the decay curve and then alternated between points at each end. In the Spiraltron runs, the digital output of the beam-current integrator was counted by a scaler preset to count a fixed amount of charge. The preset scaler controlled scalers which counted Spiraltron pulses and time in seconds. In the proportional counter runs, the computer code enabled spectra to be accumulated for preset amounts of charge. Time in seconds was also recorded by the computer. Spiraltron runs required less than 10 min/counting position. Proportional counter runs typically required several minutes per counting position. The background with beam off (dark current) was measured at several different detector positions per run for measured amounts of time. The background with beam on but with magnetic field off, was also measured at several detector positions for each run. The observed integrated beam currents for a given constant number of beam particles per second were not the same for zero field and opposite field directions. This effect was attributed to a field-dependent secondary electron collection efficiency and the different deflections of the beam. These different apparent currents were measured before and after each run so as to enable a proper normalization of the background counting rate per beam particle.

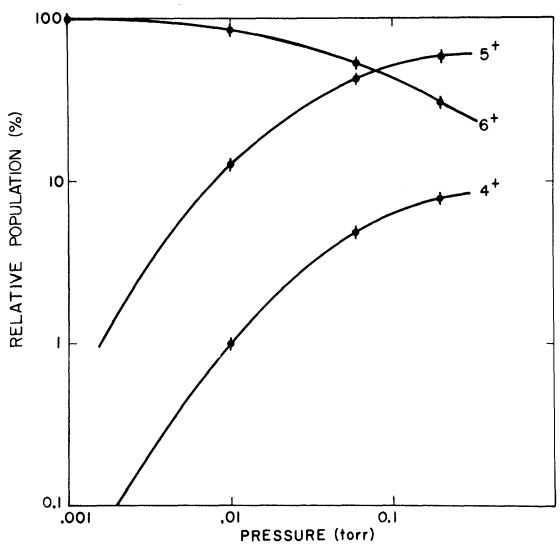

FIG. 4. Relative charge-state distributions obtained for C^{6+} at 25 MeV through argon as a function of gas-cell pressure.

IV. RESULTS

A. Metastable-Beam Formation

Figure 4 shows measured charge-state distributions beyond the windowless gas cell as a function of argon adder-gas pressure. The incident beam was 25 MeV C^{6+}. At high pressures, greater than 0.5 Torr, the relative charge-state distribution approaches equilibrium in agreement with the data of Ref. 25. Similar results were obtained at 35 MeV, and for N_2 exchange gas.

Most $2\,^2S_{1/2}$ quench-radiation decay curves were obtained at pressures near 0.1 Torr so as to keep the heliumlike component of the beam at less than 10% of the hydrogenlike component. Metastable states of heliumlike C^{4+} near 250 eV are potential major contributors to background radiation. The dominant decay modes are two-photon ($2E1$) emission from the $2\,^3S_1$ and $2\,^1S_1$ states to the $1\,^1S_0$ ground state.[26] In addition, weak higher-multipole single-quantum branches to the ground state are possible from certain high-Z heliumlike metastable states.[27] The lifetimes involved, however, are such that the number of decays per centimeter is small. The signal-to-background ratio was observed to be approximately constant within a gas-cell pressure range of 0.01–0.24 Torr corresponding to a change in the 5^+-to-4^+ ratio of 45%. In addition to radiation from C^{4+}, possible background components which might depend on adder-gas-cell pressure would be radiation generated by the increased small-angle scattering, or interactions with the greater residual gas in the quenching region. The surviving 6^+ beam, of course, contributes no atomic background radiation.

Several theoretical and experimental studies on electron pickup to high n states by fast protons in gases have been reported.[28] The theory describing the process should be applicable to high-Z hydrogenics. At beam velocities large compared with the orbital velocity of the electron being captured, for hydrogen exchange gas, as many as 12% of the C^{5+} ions might be in the $2\,^2S_{1/2}$ metastable state.[29] The total intensity would be down, however, owing to the greatly reduced total electron pickup cross section.

The actual fractional pickup to the $2\,^2S_{1/2}$ state could be extracted from the quench-radiation data provided that the absolute efficiency for detection of C^{5+} Lyman-α radiation was known. Assuming 100% efficiency for conversion of photons in the

proportional counter, an assumption warranted by the independence of count rate as proportional gas pressure was changed from 50 to 100 mm Hg, the absolute efficiency of the device is determined by the transmission of the proportional counter window at 363 eV. Using manufacturer's data,[21] we calculate a transmission of 35% at 363 eV for the Parylene-C and mesh window used. The number N_0 of metastable atoms per 5^+ ion is then given by

$$M = \frac{N_0}{I/\bar{q}} = \frac{N(x)}{2f(\sin l/\Lambda)\, d\Omega\, \epsilon} \,. \tag{19}$$

I is the integrated beam current in coulombs, $\bar{q}$ is the average ionic charge, $N(x)$ is the number of Lyman-α photons detected at the point x, l is the length of beam visible to the detector, Λ is the decay length, $d\Omega$ is the solid angle subtended by the detector, ϵ is the detector efficiency, and f is the prequenched fraction from the gas cell to the point x. The quantity f is calculated using Bethe–Lamb quenching theory, 780 GHz for the Lamb shift and the measured spatial extent and fringing of the applied magnetic field. The result at 25 MeV is $M = 0.022 \pm 0.010$ $2^2S_{1/2}$ pickup. A decrease in this fraction was noted on changing from argon to molecular nitrogen as the adder gas, but this effect was not investigated further.

Another result obtained from comparing proportional counter data with equivalent spiraltron results is the efficiency of the spiraltron electron multiplier for the 363-eV incident photons. The result is the relatively low value of about 10^{-3}.

B. Quench-Radiation Decay Curves

The value for s, the Lamb shift is determined from measured decay lengths using the formalism outlined in Sec. II above. The inherent statistical precision of any one lifetime measurement of this type is on the order of 1%. As s is proportional to the square root of the lifetime, a single measurement precision limit is about 0.5%. The decay length for any measurement, however, is controlled by varying the quenching field and/or particle velocity. Practical limitations on velocity are introduced by charge exchange considerations. Limitations on quenching field are introduced primarily by count rate and decay length considerations. At low fields, the decay length is longer than the 5.08-cm homogeneous field region and hence can be less precisely extracted from the data. At high fields, too few metastables survive passage through the several centimeter fringing field, leading to low relative count rates.

As a compromise, data was obtained at quenching fields which yielded one to three decay lengths in the measurement region. Figure 5(a) shows three decay curves taken at 25 MeV, and Fig. 5(b) shows three curves at 35 MeV. The change in slope proportional to B^2 is immediately apparent whereas the square-root dependence on energy is less obvious. Many possible systematic effects, however, are strongly energy dependent. The better statistics of Fig. 5(a) are due to the higher efficiency of the proportional counter.

The background, obtained by counting with quenching field off, has been subtracted from the points shown. Within statistics, the background was observed to be independent of detector position. For the Spiraltron runs, the background was approximately 4% of the field-on countrate at the midpoint of a 2600-G run. The corresponding figures for 2000 and 3300 G are 2 and 8%, respectively. For proportional counter runs, typical backgrounds were reduced to 3, 1.5, and 6% at the same fields. Proportional counter spectra (see Fig. 6) indicated that the background was primarily at lower energies than the carbon Lyman-α line. The proportional counter window is three times the thickness of the filter used with the Spiraltron multiplier. The reduced background, using the proportional counter is possibly due to the greater

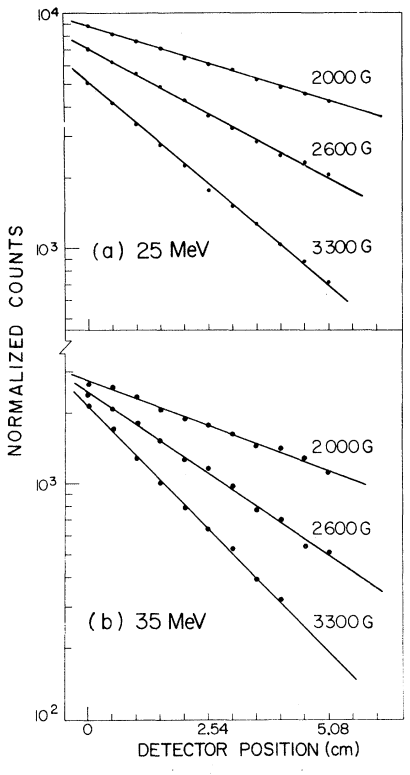

FIG. 5. Typical quench-radiation decay curves. (a) At 25 MeV using the proportional counter; (b) at 35 MeV using the Spiraltron. In both cases background counts have been subtracted. Straight lines are the best fit to the data.

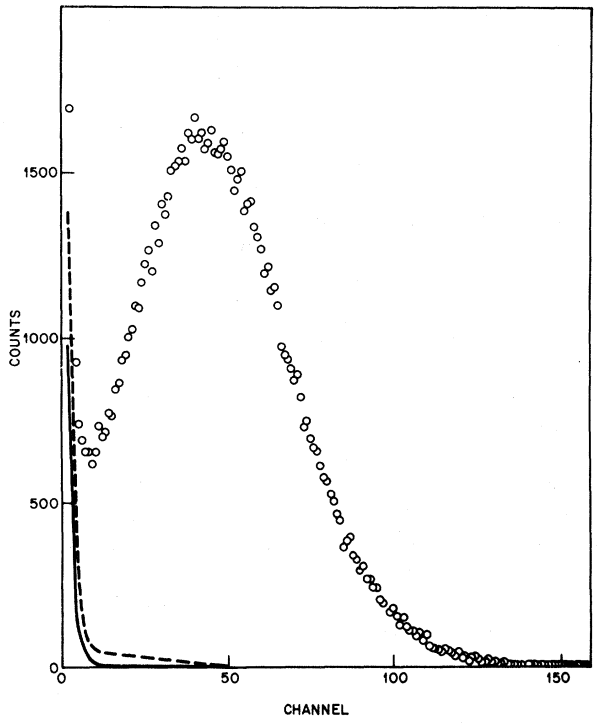

FIG. 6. Typical proportional counter pulse-height spectrum of C^{5+} Lyman-α quench radiation at position 0 (see Fig. 5). The dashed curve is the background radiation with quenching field off, and the solid curve is the dark current and electronic noise with beam off.

longer-wavelength absorption of the thicker Parylene.

The good agreement of the data of Fig. 5 with pure exponential decay is a first-order corroboration that some systematic corrections, discussed below, are small. Decay lengths taken from curves like those shown, without *any* corrections, are sufficient to define the Lamb shift to about 2%. Occasionally, points fell several standard deviations outside of the first fit to the data. Such points were always repeated with the usual result of a more consistent value. Possible explanations for the random anomalous points, are misreading of counter position, fluctuations in gas pressure, and transients in the current integration system. (The data reported in this paper were obtained with a manually positioned precision linear motion vacuum feedthrough. The apparatus has since been modified with a stepping motor interfaced to a computer-controlled data-acquisition system controlling the motion.)

Some early data were obtained normalized to a second fixed Spiraltron. The results for $\mathcal{S}$ were not changed, but the statistical fit of any one curve was poorer owing to the poor (few percent) statistics of normalization counts.

V. ANALYSIS OF RESULTS

It is desired to extract a value for $\mathcal{S}$ accurate to 1% or better from decay curves of the sort presented in Sec. IV. Hence, the general program is to consider all effects which may influence the result at the 0.1% or greater level. In Sec. II, the Bethe–Lamb quenching theory which underlies the analysis was discussed. It was shown that the metastable atoms should decay as a simple exponential in time t as they move through the quenching motional electric field. Since our atoms are moving with uniform velocity v, this appears in the laboratory as an exponential decay with position $x = vt$. Thus, to lowest order of approximation, the signal which is proportional to $dN(x)/dx$, the number of metastables decaying per unit length, may be written as

$$S_{\mathrm{Sig}}(x) = \frac{dN(x)}{dx} = P_1 \exp\left(-\frac{x}{v\tau_{2S}(P_2)}\right) , \qquad (20)$$

where P_1 and P_2 are adjustable parameters. Here we take the point of view that all quantities in Eq. (14) for τ_{2S} are known except the Lamb shift. Therefore, τ_{2S} is a function only of $\mathcal{S} \equiv P_2$. Aside from considerations of the background count rate and deflection effects, we have found that all other identifiable corrections to the simple exponential decay of Eq. (20) effect the determination of $\mathcal{S}$ at the 0.1% or smaller level. Consideration is now given to these corrections which are of order 0.1–1%.

A. Zeeman Effect

Until now, the laboratory magnetic field has been discussed only as the source of the motional electric field. The magnetic field in the moving frame ($B_{\mathrm{mov}} = \chi' B_{\mathrm{lab}}$) also gives rise to the well-known Zeeman splitting of the magnetic sublevels, thus lifting the degeneracy in the azimuthal quantum number m_j. It is easily seen that to an accuracy, more than sufficient for the present purpose, [8] one obtains

$$E_{S_{1/2}} = \mathcal{S} + 2m_j \mu_B B_{\mathrm{mov}} , \quad m_j = \pm\tfrac{1}{2}$$

$$E_{P_{1/2}} = \tfrac{2}{3} m_j \mu_B B_{\mathrm{mov}} , \quad m_j = \pm\tfrac{1}{2}$$

for the energy levels (see Fig. 7), where μ_B is the Bohr magneton. The Zeeman splitting is independent of Z, and hence becomes less important in experiments on high-Z hydrogenics. The motional electric field is transverse to the quantization axis taken in the conventional sense along the direction of B_{mov}. Consequently, because of the resulting selection rule on the electric perturbation, $\Delta m_j = \pm 1$, the α level, $m_j = \frac{1}{2}$, couples only to the f level, $m_j = -\frac{1}{2}$, and the β only to the e. There are then, in effect, two different metastable species

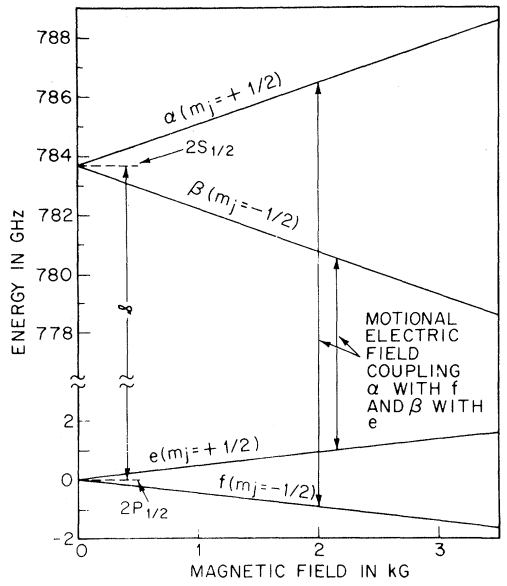

FIG. 7. Zeeman effect in the $n=2$ state of C^{5+}.

in our apparatus, the α's with δ increased slightly by $\Delta\alpha = \frac{4}{3}\mu_B B_{\text{mov}}$ and the β's with δ decreased by $\Delta\beta = -\frac{4}{3}\mu_B B_{\text{mov}}$. As a result, the two states decay at somewhat different rates Γ with

$$\Gamma_\alpha = \frac{1}{\tau_\alpha} = \frac{1}{\tau_{P_{1/2}}} \frac{|V|^2}{\hbar^2[(\delta+\Delta\alpha)^2 + 1/(4\tau_{2P}^2)]} \quad \text{and} \quad (21)$$

$$\Gamma_\beta = \frac{1}{\tau_\beta} = \frac{1}{\tau_{P_{1/2}}} \frac{|V|^2}{\hbar^2[(\delta+\Delta\beta)^2 + 1/(4\tau_{2P}^2)]} .$$

The separate modified decay rates may differ by as much as 2% from the unperturbed rate for the highest fields used.

The signal expression must also be modified,

$$S_{\text{Sig}}(x) = P_1\left[\exp\left(-\frac{x}{v\tau_\alpha(P_2)}\right) + \exp\left(-\frac{x}{v\tau_\beta(P_2)}\right)\right] \quad (22)$$

to allow for the two different decay rates. Here we have assumed that the α and β levels are excited equally.

A consequence of extracting δ values from the decay curves utilizing Eq. (22) was the realization that inclusion of the Zeeman effect does *not* effect the result significantly. This is understood by noting that the α's decay a bit more slowly because of the Zeeman effect, the β's a bit more quickly, giving a composite decay curve which is essentially unperturbed by the Zeeman effect. This conclusion is altered somewhat by considerations of prequenching.

B. Prequenching

Before reaching the uniform-field region where decay curves are obtained, the metastables must pass through the fringing magnetic field which also induces quenching. In the extreme case of high beam energy and high magnetic field, approximately 90% of the metastables are prequenched before reaching the uniform-field region. Of itself, this prequenching would not effect the decay curves. However, since the prequenching is occurring in a magnetic field, the α's and β's are prequenched at a different rate. The result is somewhat unequal population (~few percent) of the α's and β's entering the uniform-field region. Since the net effect on δ is quite small, we take the point of view that the surviving fraction of α's and β's, $F_{S\alpha}$ and $F_{S\beta}$, can be calculated by assuming the theoretical value for δ and measuring the fringing field. The expression for the signal must then be modified to allow for unequal populations of α's and β's.

For some position x in the fringing field $F_{S\alpha}$ may be obtained by integration of Eq. (19):

$$F_{S\alpha(x)} = \frac{N_\alpha(x)}{N_\alpha(x_0)} = \exp\left(-\frac{1}{v}\int_{x_0}^{x}\Gamma_\alpha(x)\,dx\right) . \quad (23)$$

The integration is taken from position x_0 where the fringing field is vanishing small. It should be noted that both the numerator and denominator of Eq. (20) for Γ_α are now functions of x as both the perturbation and the Zeeman splittings are position dependent.

In practice, the fringing field is measured with a Hall probe, and Eq. (23) is integrated numerically over a 22-cm region prior to the uniform-field region. The magnetic field is found to fall to the order of 1 G over the 22-cm distance. The signal expression is then modified to allow for prequenching as follows:

$$S_{\text{Sig}}(x) = P_1\{F_{S\alpha}\exp[-x/v\tau_\alpha(P_2)] + F_{S\beta}\exp[-x/v\tau_\beta(P_2)]\} . \quad (24)$$

C. $2^2P_{3/2}$ Level

The signal expression evolved to this point, Eq. (23), has not taken account of the presence of the $2^2P_{3/2}$ level. The same electric field which mixes the $2^2S_{1/2}$ and $2^2P_{1/2}$ levels will also mix the $2^2S_{1/2}$ and $2^2P_{3/2}$ levels, although to a much smaller extent as the inverse level separation is involved in a fundamental way (see Sec. II). Consequently, the metastables will decay more quickly than allowed for thus far. The relevant result of the three level treatment was the modification of τ_{2S} to include an additional symmetrical term with δ replaced by $\Delta E - \delta$ and V replaced by M.

Thus, the lifetimes are modified (τ_α and τ_β go to τ'_α and τ'_β) to include this term.

D. Time Dilation

One of the primary results of special relativity is the principle of time dilation. A clock moving relative to a stationary observer appears to run slow by the factor $\gamma' = (1 - v^2/c^2)^{-1/2}$. The decaying metastables are, in effect, moving atomic clocks which, because of the time dilation principle, should appear to decay less quickly according to the expression

$$\tau_{2S}(\text{lab}) = \gamma' \tau_{2S}(\text{mov}) \ .$$

Incorporating this effect along with the results of Sec. V B, we obtain a final expression for the signal

$$S_{\text{Sig}}(x) = P_1 \left[F_{S\alpha} \exp\left(-\frac{x}{v\gamma' \tau'_\alpha(P_2)} \right) + F_{S\beta} \exp\left(-\frac{x}{v\gamma' \tau'_\beta(P_2)} \right) \right]. \quad (25)$$

E. Background

The procedure followed throughout the course of the experiment has been to assume that the background count rate is independent of magnetic field and perform a background subtraction at each point on the decay curve prior to analysis. A test of this assumption was made utilizing the proportional counter decay curves. Here successive analyses of the same decay curve data were performed using a progressively higher low-energy cutoff in the photopeak sums (see Fig. 6). In this way, a series of decay curves were generated from one set of data, each having a progressively smaller background subtraction. For decay curves obtained with the low-energy threshold beyond the peak of the proportional counter spectrum, the background subtraction was negligible. No significantly different result was obtained as the low-energy threshold was varied.

F. Beam Deflection

Two assumptions, implicit in writing Eq. (25) for the signal, are that the length of beam segment viewed by the detector and the solid angle subtended by the detector are independent of position x along the beam. Both of these assumptions break down to a limited extent because of the physical deflection of the charged ion beam in the quenching magnetic field. Typically, the beam will deflect 2–3 mm in both the fringing-field and the uniform-field regions. As can be seen from Fig. 8 for the case of a downward deflecting beam, the effective solid angle is decreasing as the detector moves along the beam. Conversely, the length of viewed beam segment is increasing along the beam which tends to cancel the solid angle effect.

To put these effects on a more quantitative basis, we note that $S_{\text{Sig}}(x)$ should really be written as an integral of $dN(x)/dx$ over the finite viewed beam segment $[2l + 2\delta(x)]$ with allowance for a solid angle factor $\Omega(x)$ which may be position dependent. Thus, from Eq. (20)

$$S_{\text{Sig}}(x) = P_1 \int_{-l-\delta(x)}^{l+\delta(x)} \Omega(x') e^{x'/v\tau_{2S}} dx' \ . \quad (26)$$

Since $\Omega(x)$ is a slowly varying function of position, it may be removed from under the integral. Equation (25) is then easily integrated and a simple result obtained if it is further assumed that the shadowed regions (from l to $l+\delta$ and from $-l$ to $-l-\delta$) have on the average $\frac{1}{2}$ the effective solid angle as the unshadowed region. In this fashion, one finds

$$S_{\text{Sig}}(x) = P_1 \Omega(x) \left[\sinh\left(\frac{l}{v\tau_{2S}}\right) + \sinh\left(\frac{l+\delta}{v\tau_{2S}}\right) \right] e^{-x/v\tau_{2S}} \ ,$$

and for the case where $(l+\delta)/v\tau_{2S} \ll 1$, this becomes

$$S_{\text{Sig}}(x) = P_1 \Omega(x) [2l + \delta(x)] e^{-x/v\tau_{2S}} \ , \quad (27)$$

where P_1 is an arbitrary amplitude parameter which has absorbed all position-independent factors. Hence, the simple exponential decay of Eq. (26) is further modified by the two position-dependent factors $\Omega(x)$ and $2l + \delta(x)$. Fortunately, for the present geometry, the total effect of these factors on the exponential decay is small and modify the Lamb-shift determination by about 0.5%.

As in the case of the background subtraction, the effect of the deflection is treated as a data modification. The parameters $\Omega(x)$ and $\delta(x)$ are evaluated from measured geometrical quantities and the calculated beam deflection. The data are then corrected by these parameters prior to a nonlinear least-square fit to Eq. (27).

G. Other Corrections

In addition to the effects discussed above, numerous other possible corrections have been considered. After careful consideration and experimentation wherever possible, the following effects have been finally rejected as too small to be significant: magnetic field effect upon the detector, magnetic field gradients, NMR probe-position correction, stray electric fields, residual-gas quenching of the metastables, error in beam energy determination, contamination of C^{6+} beam with other components of the same magnetic rigidity, beam-deflection effect on the observed path length, effects associated with the exchange gas pressure and type, spontaneous decay of the metastables, and polarization of the Lyman-α radiation. High-

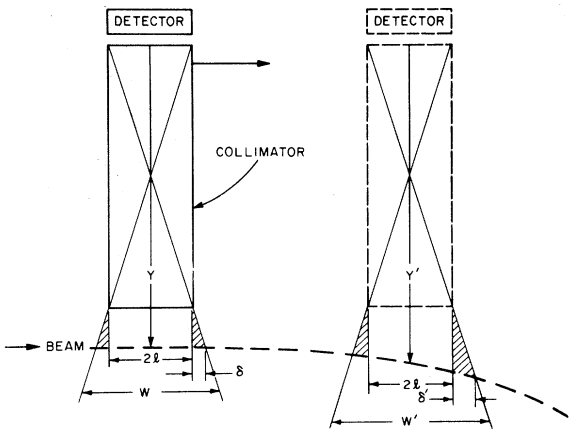

FIG. 8. Schematic representation of the effect of beam deflection on detector solid angle and viewed beam segment length.

er-order corrections to the $2^2P_{1/2}$-state lifetime, and Zeeman, relativistic, and reduced mass corrections to the matrix element V are assumed to be absent or of order $(Z\alpha)^2$.

H. Curve Fitting

A total of 21 decay curves obtained at several different magnetic fields and two beam energies were least-squares fit to Eq. (27) to give the final value for δ. The results are tabulated in Table II and plotted in Fig. 9. We find $\delta = 780.1 \pm 8.0$ GHz. Erickson's recent theoretical value of $\delta = 783.7 \pm 0.256$ GHz is in good agreement with the result. In Table III, we give a summary of the effect of all corrections on the value of δ obtained for a typical run.

TABLE II. Summary of all experimental results used to obtain the carbon Lamb shift. N and R refer to normal and reverse field directions, respectively. The first six entries were obtained with the proportional counter. In all other runs, the Spiraltron was used.

Energy (MeV)	Field (G)	Result (GHz)
24.948	2609 N	776.2 (6.0)
24.948	2610 R	774.0 (3.6)
24.948	2000 R	781.8 (5.4)
24.948	2000 N	782.7 (11.6)
24.948	3324 N	792.9 (5.0)
24.948	3325 R	772.3 (2.7)
34.979	2000 N	785.9 (10.5)
34.979	2000 R	774.2 (10.1)
34.979	3324 N	776.0 (8.3)
34.979	3324 N	782.7 (6.7)
34.979	3323 R	782.6 (7.5)
34.979	2672 N	774.6 (8.5)
34.979	2673 R	773.2 (9.9)
24.942	2676 N	770.8 (7.7)
24.942	2676 R	781.9 (10.8)
24.942	3323 N	770.0 (4.7)
24.942	3324 R	775.4 (4.8)
24.942	2000 R	802.3 (10.0)
24.942	2000 N	790.6 (16.8)
34.970	2612 N	782.2 (7.8)
34.970	2612 R	780.8 (8.5)

VI. ERROR ANALYSIS

A. Statistics

The solid lines of Fig. 5 are the best fits to Eq. (26) with two adjustable parameters, a normalization and the Lamb shift δ. The nonlinear least-squares-fitting routine of Marquardt[30] was used. The error bars on each of the 21 independent mea-

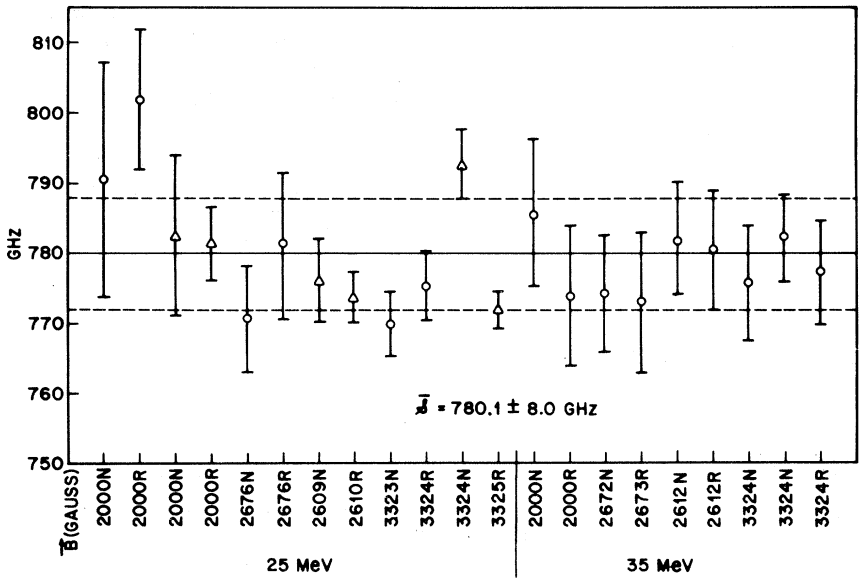

FIG. 9. Graphical representation of the data of Table II. N and R refer to normal and reverse field directions, respectively. Points indicated by triangles were obtained using a proportional counter for Lyman-α detection.

TABLE III. Summary of the effect of all corrections to a single exponential decay, on the Lamb-shift value, obtained from a typical run. The data below are for the 15th run listed in Table II.

Correction	Magnitude (GHz)
Background	−10.17
Deflection (solid angle)	+9.13
Deflection (segment width)	−4.69
$P_{3/2}$ state	+2.68
Special relativity	+0.89
Zeeman effect–prequenching	−0.09
Total	−2.25

surements of Fig. 9 represent one standard deviation (68% confidence) allowing for the small parameter correlation, assuming that the model used is correct, and that the errors are Gaussian. In the fitting routine, each datum is weighted inversely to its relative statistical error.

Though statistical errors for S vary by as much as a factor of 2 from point to point, our final result is taken as the unweighted mean, 780.1 GHz. The rational for this procedure is based on the fact that systematic errors, discussed below, are more important in the runs with low statistical errors than those with high. The higher statistical errors are associated with lower field runs, where the background and deflection corrections were smallest. We have assumed that the errors of measurement are independent of each other and are distributed normally about zero. They have been estimated, and added in quadrature with the standard error of the mean, 4 GHz, to obtain an overall standard deviation. The final value is $S = 780.1 \pm 8.0$ GHz.

B. Background

The background counts subtracted from the data of Fig. 5 was obtained with the quenching field off, all other conditions remaining constant. It was observed to be independent of position and was statistically defined to about ± 10%. Assuming this to be the *true* background it is observed to be a relatively small fraction of the typical signal count rate. The true background is defined here as counts with magnetic field on but quenching turned off. That consistent results are obtained in high fields, i.e., short decay lengths, supports the contention that the background is handled correctly. The experiment is designed, however, such that the true background cannot be measured. One approximation to that condition was obtained by counting with field on but adder gas off, i.e., essentially the 6^+ beam. The background under these conditions was less than the field off, gas on background. Further experience with high-energy oxygen beams leads us to believe that one source of background is scattered radiation produced when the particle beam stops in the Faraday cup.

We conservatively estimate the *average* uncertainty in background to be ± 50%. Such an uncertainty was shown to change an intermediate slope decay curve determination of S by ± 5 GHz which is taken as the estimated background contribution to the total uncertainty.

C. Geometric Uncertainties

Geometric uncertainties effect the determination of S in several ways. The uncertainty in counter position is negligible, less than 1 part per thousand. The uncertainties associated with particle beam size and beam axis to counter axis alignment are more subtle and do cause additions to the final quoted error. Corrections to the data for beam deflection described in Sec. V F result in an average ± 5-GHz correction to S where the ± sign is determined by the beam deflection up (−) or down (+). There is a ± 1.5-mm uncertainty in centering the 3-mm-diam beam on the 11-mm-wide detector collimator and a ± 0.5° uncertainty in aligning the detector motion with the beam direction and perpendicular to the magnetic field. These uncertainties are estimated to add ± 4 GHz to the final result.

D. Other Systematic Errors

Implicit in the geometric analysis is the assumption of uniform beam density. If this assumption is wrong, and a beam halo exists *and* there is maximal displacement of the beam axis, the Lamb shift might be systematically increased or decreased depending on the direction of the misalignment. Though the beam line was optically aligned before each run, a contribution to the total uncertainty of ± 2 GHz is estimated for this effect. Errors in quenching field and energy determination effect the result by at most ± 1 GHz.

In summary, we combine in quadrature 4-GHz statistics, 5-GHz background, 4-GHz geometry, 2-GHz halo effect, and 1 GHz for field and energy determination to obtain a final standard deviation of ± 8 GHz.

VII. CONCLUSIONS

The experimental results demonstrate the feasibility of high-Z Lamb-shift measurements by the method of fast beam, metastable quenching in a motional electric field. A result for $^{12}C^{5+}$ has been obtained which is in excellent agreement with the QED calculation of S. The accuracy of ± 1% is sufficient to allow interesting comments on Erickson's recent calculation of higher-order terms as well as on the canonical truncated ex-

TABLE IV. Partial breakdown of series-expansion calculation of Lamb shift. The formulation of Ref. 14 with the corrections of Ref. 1 was used.

Term		S H(MHz)	S C^{5+}(GHz)
2nd-order self-energy and vacuum polarization	$\alpha(Z\alpha)^4$	1050.55	733.59
Remainder	$\alpha(Z\alpha)^5$	7.14	55.52
	$\alpha(Z\alpha)^6$	−0.38	−8.06
4th-order self-energy and vacuum polarization	$\alpha^2(Z\alpha)^4$	0.11	0.14
Recoil		0.36	0.19
Nuclear size		0.13	1.49
S (Total)		1057.91	782.87

pansion. Table IV presents a partial breakdown of the usual series expansion with numerical values for hydrogen and hydrogenic carbon. The $\alpha(Z\alpha)^6$ term which is only 0.04% of the total Lamb shift for hydrogen is 1.02% for C^{5+}, the order of our uncertainty. In Erickson's formulation, the total higher-order contribution to the C^{5+} Lamb shift amounts to 6.2%, in agreement with our result. The corresponding value for hydrogen is 0.6%.

Our result may also be interpreted as verification of the nonrelativistic $2P$-state lifetime in C^{5+} to an accuracy of ± 2%, and of the Bethe–Lamb quenching theory which was employed in deriving a Lamb-shift result from the data. The accuracy of the result is determined primarily by the uncertainty in various systematic experimental effects predominently background and beam deflection. An ultimate accuracy of some small fraction of 1% should be achievable as a greater mastery of the systematics is developed.

Direct extension of the method to more highly ionized species should be feasible, provided sufficient beam energy is available for stripping the ions. It would appear now that the ultimate limitation on how far in Z the method is applicable will be set by the loss in metastability of the $2S$ state ($\tau_{2S} \propto Z^{-6}$) and by the gross beam deflection which will ensue as the large required quenching fields are applied.

We are presently in the process of extending our measurements to O^{7+} and F^{8+}. An accuracy of some fraction of 1% is anticipated which may allow more definitive comment upon Erickson's work.

ACKNOWLEDGMENTS

We thank W. L. Brown and G. M. Temmer for their enthusiastic support and encouragement, J. Gersten and I. Sellin for helpful discussion, and G. Erickson for results of calculations prior to publication. We are also indebted to J. P. F. Sellschop for collaboration in early data acquisition and R. Boie for technical assistance. R. C. Peterson and the Rutgers-Bell tandem staff constructed and installed the post stripper box and aided in developing the C^- beam.

*Supported in part by the National Science Foundation.

[1]T. Appelquist and S. J. Brodsky, Phys. Rev. Letters 24, 562 (1970).

[2]J. C. Wesley and A. Rich, Phys. Rev. A 4, 1341 (1971).

[3]S. J. Brodsky, in *Precision Measurements and Fundamental Constants*, edited by D. N. Langenberg and B. N. Taylor, Natl. Bur. Std. Spec. Publ. 343 (U. S. GPO, Washington, D. C., 1970).

[4]B. E. Lautrup, A. Peterman, and E. deRafael, Phys. Repts. 3C, 193 (1972).

[5]V. W. Hughes, in *Proceedings of the International Conference on Atomic Physics, New York* 1968, edited by B. Bederson, V. W. Cohen, and F. M. J. Pichanick (Plenum, New York, 1969), p. 15.

[6]G. W. Erickson and D. R. Yennie, Ann. Phys. (N.Y.) 35, 271 (1965).

[7]G. W. Erickson, Phys. Rev. Letters 27, 780 (1971).

[8]W. E. Lamb and R. C. Retherford, Phys. Rev. 79, 549 (1950).

[9]M. Leventhal and D. E. Murnick, Phys. Rev. Letters 25, 1237 (1970).

[10]D. E. Murnick, M. Leventhal, and H. W. Kugel, Phys. Rev. Letters 27, 1625 (1971).

[11]C. Y. Fan, M. Garcia-Munoz, and I. A. Sellin, Phys. Rev. 161, 6 (1967).

[12]B. Donnally and I. Sellin, in *Beam Foil Spectroscopy*, edited by S. Bashkin (Gordon and Breach, New York, 1968), p. 451.

[13]G. W. Erickson (private communication).

[14]B. N. Taylor, W. H. Parker, and D. V. Langenberg, Rev. Mod. Phys. 41, 375 (1969).

[15]H. A. Bethe and E. E. Salpeter, in *Handbuch der Physik*, edited by S. Flügge (Springer-Verlag, Berlin, 1957), Vol. XXXV, p. 371.

[16]G. Breit and E. Teller, Astrophys. J. 91, 215 (1940); S. Klarsfield, Phys. Letters 30A, 382 (1969).

[17]H. A. Bethe and E. E. Salpeter, in Ref. 15, p. 334.

[18]G. Feinberg (private communication).

[19]A recent discussion of other methods for calculating quenched metastable decay rates is given by C. E. Johnson, Bull. Am. Phys. Soc. 17, 454 (1972); and Helen K. Holt and I. A. Sellin, Phys. Rev. A 6, 508 (1972).

[20]J. B. Marion and C. F. Young, *Nuclear Reaction Analysis* (North-Holland, Amsterdam, 1968), p. 41.

[21]M. A. Spivak, Rev. Sci. Instr. 41, 1614 (1970).

[22]V. S. Nikolaev, Usp. Fiz. Nauk 85, 679 (1965) [Sov. Phys. Usp. 8, 269 (1965)].

[23]S. Bashkin, *Beam Foil Spectroscopy* (Gordon and Breach, New York, 1968).

[24]J. R. Oppenheimer, Phys. Rev. 31, 349 (1928).
[25]F. W. Martin, Phys. Rev. 140, A75 (1965).
[26]G. W. F. Drake, G. A. Victor, and A. Dalgarno, Phys. Rev. 180, 25 (1969).
[27]I. A. Sellin, M. Brown, W. W. Smith, and B. Donnally, Phys. Rev. A 2, 1189 (1970); R. Marrus and R. W. Schmieder, Phys. Rev. Letters 25, 1689 (1970).
[28]R. H. Hughes, E. D. Stokes, Song-Sik Choe, and T. J. King, Phys. Rev. A 4, 1453 (1971); D. H. Crandall and D. H. Jaecks, *ibid.* 4, 2271 (1971).
[29]J. Jackson and M. Schiff, Phys. Rev. 89, 359 (1953).
[30]D. W. Marquardt, J. Soc. Ind. Appl. Math. 11, 431 (1963).

PHYSICAL REVIEW A VOLUME 6, NUMBER 4 OCTOBER 1972

Energy Levels of Hydrogenlike Atoms in a Magnetic Field

H. C. Praddaude
*Francis Bitter National Magnet Laboratory,**
Massachusetts Institute of Technology, Cambridge, Massachusetts 02139

(Received 7 April 1972)

A new expansion of the wave function in Laguerre polynomials for hydrogenlike atoms in a magnetic field has been developed. This expansion reduces the Schrödinger equation to an infinite set of algebraic equations for which a fast, accurate, and unambiguous calculation of the bound states of a hydrogen atom in a magnetic field is possible. Four quantum numbers (K, C, M, N) are used to label the energy levels of the system in cylindrical coordinates. When the magnetic field is zero, the new labeling of the states is equivalent to the standard (n, l, m) quantum numbers obtained for the Coulomb potential in spherical coordinates. Numerical results are presented for the first 14 energy levels with principal quantum number $n = 1, 2, 3$. Several energy-level crossings occur in the region $0 < \gamma < 1$, where $\gamma = \hbar\omega_c/2\mathcal{R}$ and $\mathcal{R}$ is the effective Rydberg energy.

Calculations of the energy levels of hydrogenlike atoms in a magnetic field are essential for many problems in solid-state physics involving excitons or shallow donors. This paper presents a new method of calculating the bound energy levels, the general form of the wave functions, and uniquely labels the discrete energy levels of hydrogenlike atoms in a magnetic field.

In semiconductors, with relative static dielectric constants κ from 10 to 50 and effective-mass ratios from 0.01 to 0.1, the strength of the magnetic field relative to the Coulomb energy $\gamma = \hbar\omega_c/2\mathcal{R}$ ranges between 0.5 to 1000 for $B = 10T$. Here the cyclotron frequency is $\omega_c = eB/m$ and the effective Rydberg is $\mathcal{R} = Ze^4m/(32\pi^2\kappa^2\hbar^2)$. For values of γ between 0 and 1 the bound Coulomb energy levels lose their identity because of the strong admixture of levels necessary to satisfy the perturbed Schrödinger equation. For values of $\gamma \gg 1$ the binding effect of the magnetic field in the xy plane is so large that an adiabatic approximation is appropriate.[1-4] Larsen[5] and Pokatilov and Rusanov[6] have performed variational calculations for $0 \leq \gamma \leq 3$, for the first few lowest levels. Recently Cabib, Fabri, and Fiorio[7] have integrated the Schrödinger equation numerically and obtained very accurate values for the $1s$ and $2s$ energy levels for $\gamma \leq 5$. These calculations did not answer two pressing questions: (i) How does one classify and label the bound energy levels? (ii) What is the general form of the wave function? Satisfactory answers to both questions are present here. I outline the calculation here and present some of the results in tabulated and graphical form. An extensive report containing more detailed results is being prepared for publication.

The Hamiltonian for this problem is

$$H = (1/2m)(\vec{p} + \tfrac{1}{2}e\vec{B}\times\vec{r})^2 - Ze^2/(4\pi\kappa r) \quad . \tag{1}$$

It is well known that the above Hamiltonian is invariant with respect to arbitrary rotations around an axis which contains the Coulomb center and is parallel to the direction of the applied magnetic field $\vec{B}$. Therefore, the projection of the angular momentum along the direction of $\vec{B}$ is conserved. Using the cylindrical coordinates (ρ, φ, z), with the origin on the Coulomb center $+Ze$ and the z axis along the direction of the magnetic field $\vec{B}$, the angular dependence of the wave function can be separated out,

$$\Phi(\phi) = (2\pi)^{-1/2}e^{iM\Phi} \quad .$$

The z component of the angular momentum is $L_z = \hbar M$, and the quantum number $M = 0, \pm 1, \pm 2, \ldots$. Defining the effective Rydberg as the unit of energy, γ as the unit of magnetic field, and $a = 8\pi\kappa\hbar^2/(Ze^2m)$ as the unit of length, the Schrödinger equation reduces to the well-known form

$$\left[\frac{\partial^2}{\partial\rho^2} + \frac{1}{\rho}\frac{\partial}{\partial\rho} + \frac{\partial^2}{\partial z^2} - \frac{M^2}{\rho^2} - 4\gamma^2\rho^2\right.$$